Investigating the release and flow of snow avalanches at the slope-scale using a unified model based on the material point method

Johan Gaume[a,b,*], Alec van Herwijnen[b], Ted Gast[c,d], Joseph Teran[c,d], Chenfanfu Jiang[d,e]

[a] SLAB Snow and Avalanche Simulation Laboratory, Swiss Federal Institute of Technology EPFL, Lausanne, Switzerland
[b] WSL Institute for Snow and Avalanche Research SLF, Davos, Switzerland
[c] University of California Los Angeles, USA
[d] Jixie Effects, Los Angeles, USA
[e] University of Pennsylvania, Philadelphia, USA

A B S T R A C T

Snow slab avalanches start with a failure in a weak snow layer buried below a cohesive snow slab. After failure, the very porous character of the weak layer leads to its volumetric collapse and thus closing of crack faces due to the weight of the overlaying slab. This complex process, generally referred to as anticrack, explains why avalanches that release on steep slopes can be triggered from flat terrain. On the basis of a new elastoplastic model for porous cohesive materials and the Material Point Method, we investigate the dynamics of mixed-mode anticracks, the subsequent detachment of the slab and the flow of the avalanche. In particular, we performed two and three dimensional slope scale simulations of both the release and flow of slab avalanches triggered either directly or remotely. We describe the fracture and flow dynamics on a realistic topography and focus on the volumetric plastic strain, stress invariants, propagation speed and flow velocity. Our simulations reproduce typical observations of "en-echelon" fractures and the propagation speed reached up to three times that measured in field experiments. In addition, slab fracture always started from the top in the Propagation Saw Test while it systematically initiated at the interface with the weak layer at the crown of slope-scale simulations in agreement with limited field observations. During the avalanche flow, snow granulation, erosion and deposition processes were naturally simulated and do not need additional implementations. Our unified model represents a significant step forward as it allows simulating the entire avalanche process, from failure initiation to crack propagation and to solid-fluid phase transitions, which is of paramount importance to forecast and mitigate snow avalanches.

1. Introduction

Snow is a complex material which can sustain stresses like a solid or flow like a fluid depending on the applied loading and strain rate (Louchet et al., 2013). The solid-fluid transition in snow can have dramatic consequences such as snow slab avalanches which are responsible for most of the damage and fatalities related to avalanches. Although slab avalanches can be devastating phenomena of large scale (> 100 m), their release is controlled by failure mechanisms at the microscopic scale (< 1 mm) in the snowpack. It is thus intrinsically a multiscale issue. Snow slab avalanches result from a sequence of fracture processes including (i) failure initiation in a weak layer underlying a cohesive snow slab, (ii) the onset of crack propagation, (iii) dynamic crack propagation through the weak layer across the slope, and (iv) detachment and sliding of the slab, followed by the flow of the avalanche (Schweizer et al., 2003).

Our understanding of the mechanical properties of snow as well as slab avalanche release processes has improved over the last years (Schweizer et al., 2016). This progress is related to modern experimental methods coupled with multiscale models, which were encouraged by the fast increase of computational capabilities. In particular, laboratory experiments and simulations based on X-ray microtomography highlighted the mixed-mode nature of snow failure including tensile, shear and compression failure modes (Hagenmuller et al., 2015; Reiweger et al., 2015; Chandel et al., 2015; Hagenmuller, 2017; Srivastava et al., 2017). The typical anisotropic microstructure of persistent weak layers leads to lower strengths in shear than in compression (Reiweger and Schweizer, 2010).

Concerning crack propagation, the pioneering work of McClung (1979) (strain-softening shear failure model) showed that a slab avalanche is actually more complex than just assessing whether the stress due to the slab load is larger than the weak layer strength. It is a

---

complex fracture mechanical problem. The development of the Propagation Saw Test (PST) by Sigrist and Schweizer (2007) and Gauthier et al., (2008) confirmed the latter observation but also changed our view on slab avalanche processes. van Herwijnen and Jamieson (2005) highlighted the importance of the structural collapse of the weak layer after failure as well as the crucial influence of slab elasticity and strength. Indeed, if a local failure is induced in the weak layer by damage accumulation at the bond scale, its porous character induces a volumetric collapse and thus closing of crack faces (Heierli et al., 2008; Gaume et al., 2017a) generally referred to as anticrack. The resulting slab deformation (bending and stretching) induces local stress concentrations in the weak layer. The onset of crack propagation occurs if the crack length exceeds the so-called critical crack length or if the load at the crack tip becomes critical, which can occur even if the average stress due to the slab is lower than the weak layer strength (knock-down effect, Schweizer, 1999; Gaume et al., 2014). On the other hand, slab deformation induces large tensile forces in the slab which can fracture and thus prevent further propagation in the weak layer (Gaume et al., 2015; Benedetti et al., 2019; Reuter and Schweizer, 2018). Coupled with particle tracking velocimetry (PTV), the PST allowed scientists to derive the crack propagation speed also in addition to other relevant mechanical properties such as the elastic modulus of the slab (van Herwijnen et al., 2016a, b). Recently, Gaume et al. (2015, 2017) developed a discrete element model which reproduces the onset and dynamics of fractures in weak snow layers at the scale of a PST field test. It was shown in particular that the crack propagation speed, which depends on snowpack properties, strongly influences the propagation distance (van Herwijnen et al., 2016b).

While the research conducted on avalanche formation in the past decade (Schweizer, 2017) allowed to better grasp the physical ingredients required for release of an avalanche (Reiweger et al., 2015; Schweizer et al., 2016; Bair et al., 2016; Gaume et al. 2017; Gaume et al., 2018a; Mulak and Gaume, 2019), numerical modeling of avalanche dynamics and different flow regimes (Sovilla et al. 2008; Köhler et al., 2018) is still strongly debated (Issler et al., 2018; Bartelt and Buser, 2018; Ancey, 2018). The bottleneck comes from three main aspects: i) the oversimplified Voelmy rheology which fails to reproduce the observed friction which has to be empirically calibrated (Ancey et al., 2004; Jamieson et al., 2008; Gauer and Kristensen, 2016) leading to numerical errors at the avalanche front (Ancey, 2018); ii) the depth-averaging which excludes important vertical flow features including snow granulation (Steinkogler et al., 2015) which influence avalanche velocity, runout and pressure (Harbitz et al., 1998; Jamieson et al., 2008); iii) the release zone is empirically evaluated. With recent increases in computational

capabilities, it seems that current depth-averaged avalanche dynamics models could now evolve towards a full three-dimensional approach including more realistic and history-dependent snow mechanical models to account for transitions in flow regimes (Köhler et al., 2016, 2018).

Classical numerical methods used in snow science such as DEM (Discrete Element Method, e.g. Hagenmuller et al., 2015), FEM (Finite Element Method, e.g. Podolskiy et al., 2013) or FV (Finite Volumes, e.g. Christen et al., 2010) fail to model the entire avalanche process, from quasi-static failure initiation to dynamic crack propagation and flow at the slope scale. In contrast, the Material Point Method (MPM, Sulsky et al., 1995) is a continuum and hybrid Eulerian-Lagrangian method which has the advantage of dissociating Lagrangian material particles and Eulerian calculation points allowing it to be an ideal candidate for modeling fractures, collisions and coexistence between solid- and fluid-like behaviors. Indeed, the collective behavior (friction and collisions) of fractured solid materials can lead to a viscous fluid aspect at the macroscopic scale.

Here, we conducted numerical simulations based on MPM and a finite strain elastoplastic constitutive model for porous cohesive materials which accounts for cohesion softening and volume reduction to simulate the weak layer. Our new model accurately reproduces the onset and dynamics of propagating anticracks monitored in snow fracture experiments and is able to simulate both the release and flow of slab avalanches at the slope scale in three-dimensions (Gaume et al., 2018a). The main difference in the model compared to Gaume et al. (2018a) consists in the introduction of a new weak layer parameter allowing us to independently control the internal friction and the dynamic friction after failure.

2. Methods

2.1. The Material Point Method (MPM)

MPM consists in using particles (material points) to track mass, momentum and deformation gradient. The Lagrangian character of these quantities facilitates the discretization of the mass conservation equation as well as the acceleration term in the momentum conservation equation. However, the lack of mesh connectivity between particles complicates the calculation of spatial derivatives of the stress tensor. Hence, this is done by using a regular background Eulerian grid mesh and interpolation functions over this grid in the standard FEM manner using the weak form. We will closely follow the explicit MPM algorithm from Stomakhin et al. (2013) with a symplectic Euler time integrator. The primary difference is the elastoplastic constitutive model (see below) regarding how stress is computed and processed

Fig. 1. Three dimentional simulation of a real-scale snow slab avalanche.

under the plastic flow. We refer to Jiang et al. (2016) and Gaume et al. (2018a) for more details about the MPM time stepping algorithm.

2.2. Finite strain elastoplastic model

The mechanical model is described in detail in Gaume et al. (2018a). We summarize the main characteristics below.

For both the slab and the weak layer, we use a mixed-mode shear-compression yield surface in agreement with laboratory experiments (Reiweger et al., 2015) and simulations based on X-ray computed tomography (Hagenmuller et al., 2015; Chandel et al., 2015; Hagenmuller, 2017; Srivastava et al., 2017). The yield surface is defined in the space of the p-q invariants of the stress tensor. The pressure p is given by $p = -\text{tr}(\tau)/d$, where d is the problem dimension and τ is the Kirchhoff stress tensor. The Mises stress q is given by $q = (3/2 \, \mathbf{s} : \mathbf{s})^{1/2}$ where $\mathbf{s} = \tau + p\mathbf{I}$ is the deviatoric stress tensor ($\mathbf{I}$ is the identity matrix). We use the following cohesive cam clay yield surface proposed by Gaume et al. (2018b):

$$y(p, q) = (1 + 2\beta)q^2 + M^2(p + \beta p_0)(p - p_0) \tag{1}$$

in which p_0 is the isotropic compressive strength, M is the slope of the critical state line and characterises the internal friction and βp_0 is the isotropic tensile strength in which β characterises cohesion. When $y(p,q) \leq 0$ the material is elastic and follows Hook's law (with a Young's modulus E and Poisson's ratio ν).

At failure ($y(p,q) > 0$), hardening and softening is performed by expanding or shrinking the yield surface, respectively, through variations in p_0. For the slab, compression leads to hardening, promoting compaction, while tension leads to softening, promoting fracture. Hardening or softening depends on the volumetric plastic strain ϵ_V^P according to:

$$p_0 = K \sinh(\xi \max(-\epsilon_V^P, 0)) \tag{2}$$

in which K is the bulk modulus and ξ is the hardening factor.

For the porous weak layer, the hardening rule of the slab was modified to allow softening and collapse under compression. At failure p_0 decreases according to

$$p_0 = K \sinh(\xi \max(-\eta, 0)) \tag{3}$$

where η is the anticrack plastic strain defined as

$$\dot{\eta} = \begin{cases} \alpha |\dot{\epsilon}_V^P|, & \text{if } t \leq t_c \\ \dot{\epsilon}_V^P, \beta = 0, M = M_d & \text{if } t > t_c \end{cases} \tag{4}$$

where α is the softening factor controlling the weak layer toughness (or fracture energy) and t_c is the time when $p_0 = 0$. Once stresses reach zero, cohesion is removed and a standard hardening rule (Eq. 2) is used leading to a purely frictional/compaction behaviour (Gaume et al., 2018a). The only difference with the model presented in Gaume et al. (2018) consists in the implementation of a different friction parameter M_d after complete softening. Hence, M characterises the internal friction and M_d controls the dynamic (or crack-face) friction parameter and two different values can be provided. This allows to account for the fact that the internal friction of snow is generally lower than the dynamic friction (Reiweger et al., 2015; van Herwijnen et al., 2010). After softening, the yield surface of the weak layer thus reads

$$y(p, q) = q^2 + M_d^2(p^2 - pp_0) \tag{5}$$

This new softening rule mimics bond breaking in the weak layer and subsequent grain rearrangement leading to volumetric collapse due to the compressive weight of the overlaying snow slab. Physically, this mechanical behavior is related to the fact that even under compression, the solid matrix of porous solid is mostly under tension and shear (Gaume et al., 2017b).

2.3. Simulated geometries and mechanical parameters

Our model was already presented and validated using data of the Propagation Saw Test (PST, van Herwijnen et al., 2010, 2016) in Gaume et al. (2018a). Hence, here we will focus on the analysis of slope-scale simulations. First, we modelled a two dimensional slope (Fig. 2) of length $L = 25$ m and height $H = 13$ m with a constant slab depth $D = 0.4$ m. The maximum slope angle is 45°. For three dimensional simulations (Figs. 1 and 2), the geometry was chosen to mimic a concave slope with a maximum snow depth in the middle of the path. It was reported by Vontobel et al. (2013) that this type of slope shape was most commonly associated with avalanches. The length $L = 22$ m and height $H = 9$ m. Spatial variability of snow depth was added with using a simplex Perlin terrain noise model (Perlin, 2002) with a resulting standard deviation of ~25% and correlation length ~10 m (Schweizer et al., 2008; Helbig et al., 2015). The mechanical parameters are presented in Gaume et al. (2018a). Finally, we simulated a larger system size in two-dimensions (Fig. 2, bottom) with a length $L = 480$ m and height $H = 180$ m including some ground
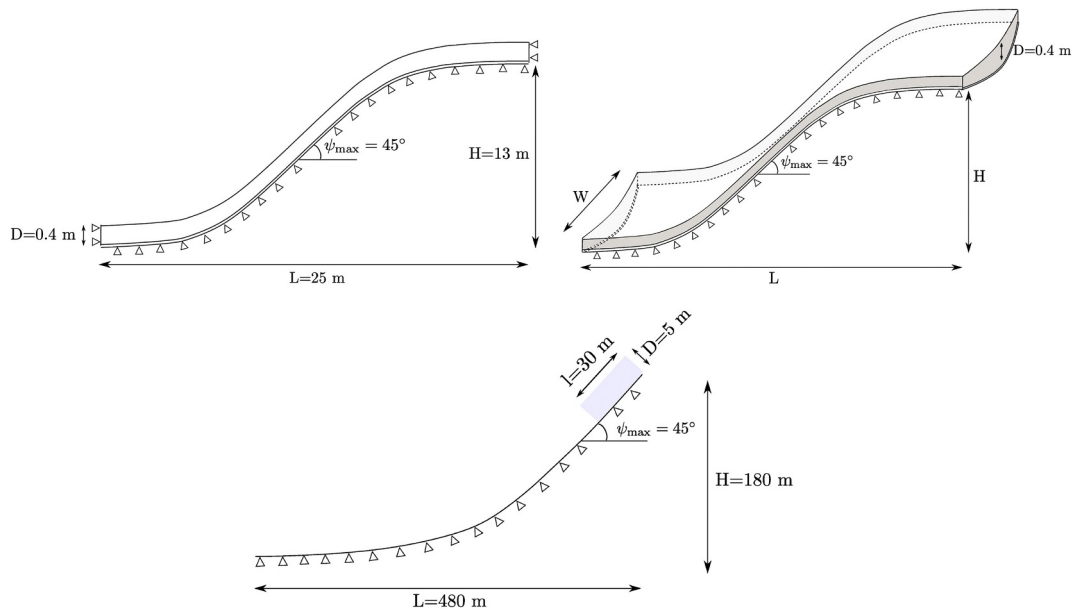

Fig. 2. Geometry and boundary conditions of the 2D (top left), 3D (top right) and large scale 2D (bottom) simulated systems.

roughness (simplex Perlin terrain noise). In this case, we only simulated the flow of a 30 m long and 5 m thick rectangular snow volume on a frictional surface (friction coefficient of 0.4) with the same mechanical properties as the slab in the 2D slab avalanche simulation.

3. Results

3.1. Avalanche release

In both 2D and 3D cases, we simulate the remote triggering of a slab avalanche by a snowman (in blue in Fig. 3). The snowman initiates a failure in the weak layer which then propagates along the slope as a mixed-mode anticrack. The collapse of the weak layer around the snowman induces local slab fractures similar to the "shooting cracks" often observed in the field (Fig. 3 and Fig. A1 in the appendix). We observe "en-echelon" types fractures (Gauthier and Jamieson, 2010) i.e. crack propagation in the weak layer is subsequently followed by slab fractures slightly down slope the crack tip, as shown in Fig. 3 in 2D and Fig. A1 in 3D (appendix). These en-echelon slab fractures occur in steep parts of the slopes and the distance between the tensile crack in the slab and the crack tip in the weak layer is found to be < 1 m in our simulations. In 3D (Fig. A1), the subsequent en-echelon fractures are not perfectly perpendicular to the slope due to the slope concavity. Ultimately, this leads to the somewhat jagged (not perfectly straight nor mesh aligned) character of the flanks observed in nature.

In addition, the crack propagation speed was evaluated based on the anticrack plastic strain. The crack tip was defined as the location of the transition for which the anticrack plastic strain η became non-zero. The crack propagation speed was then evaluated by tracking the crack tip in time. The average crack propagation speed was found around 62 m/s but locally increased in steep parts of the slope where the propagation speed reached 140 m/s. In the 2D simulation (Fig. 3), we observe that the crack started to propagate a few meters ahead of the snowman, then stopped, and then propagated again. Although the crack propagation speed reached its maximum value close to the maximum slope angle, crack propagation speed cannot be explained by slope angle alone. In fact, crack propagation speed was strongly influenced by changes in slope angle and thus by the local curvature. Whereas convexities (close to the snowman) lead to a reduction of the crack speed, concavities (top of the slope) lead to a significant increase in crack propagation speed. Furthermore, crack propagation speed was influenced by slab tensile fractures (Fig. 3) as it typically decreases when the crack tip reaches approximately 1 m ahead of a slab fracture. In 3D (Fig. 4 and Fig. A1), we observed the same general features, i.e. an average crack propagation speed around 60 m/s and local speeds reaching up to 130 m/s. The propagation speed was also larger at concavities than at convexities. We also observed local surges of propagation followed by a decrease in propagation speed (Fig. 4) which coincide with locations of slab fractures (Fig. A1). Finally, propagation in the anti-plane direction was approximately twice slower than in the slope direction. This is highlighted in Fig. A1 in which we clearly see the preferred propagation direction in the up-slope direction (transition from a circle plastic zone shape zone during failure initiation shape to an elongated one during propagation).

Once the crack in the weak layer propagated across the slope, the slab released where the slope angle exceeded the friction angle of the weak layer. The upslope section of the fracture line, or "crown" fracture started branching from the bottom of the slab at the interface with the
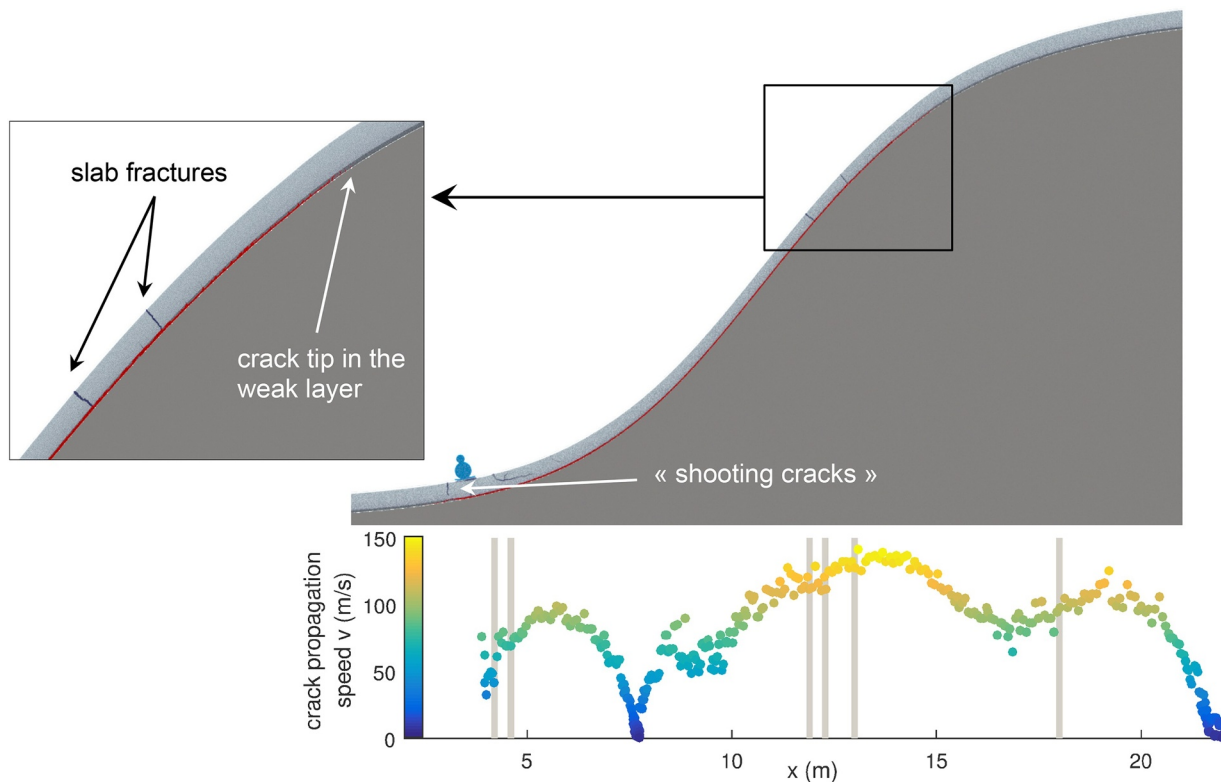

Fig. 3. Top: Simulation of remote avalanche triggering with shooting cracks and en-echelon fractures. Bottom: Crack propagation speed along the slope. The grey bars correspond to the location of slab fractures.
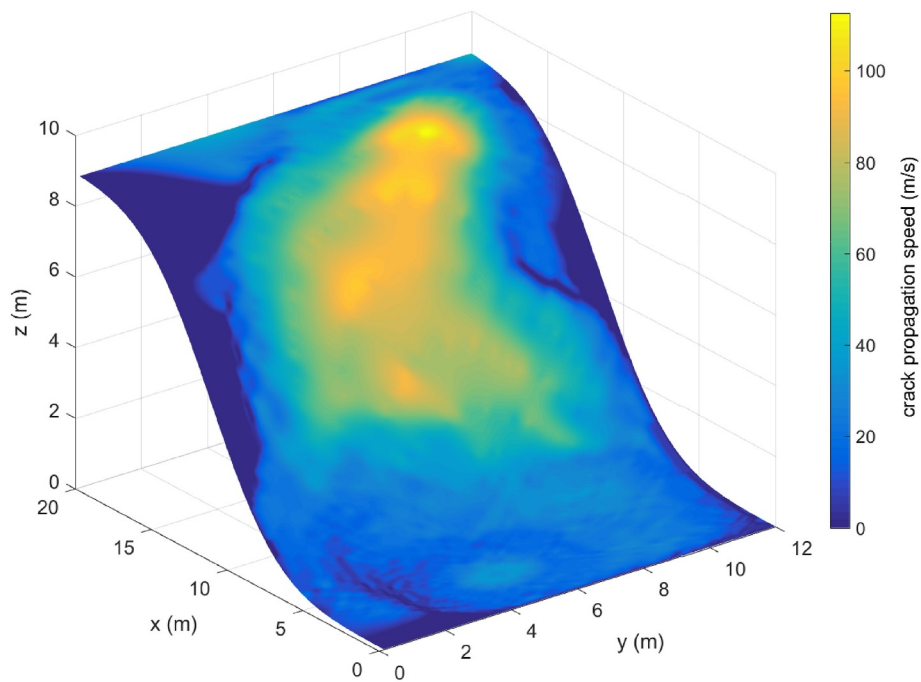
Fig. 4. Crack propagation speed in 3D.

weak layer as shown in Fig. 5. This contrasts with the slab fracture in PST experiments which systematically started branching from the top, in MPM simulations and experiments (Gaume et al., 2018a, Fig. 5). Finally, as shown in Fig. 1 and by Gaume et al. (2018a), the release zone has an arc crown line, jagged flanks and staunchwall which are commonly observed (Perla, 1971). In the slab, the crown fracture occurs in tension and is followed by the staunchwall and flank shear fractures.

3.2. Avalanche flow dynamics

For slab avalanche simulations, the crown, staunchwall and flanks (in 3D) fractures are followed by sliding of the slab on the broken weak layer. The slab then slides over the staunchwall shear crack and then over the section of the slab which did not slide. Although the slabs we simulated are quite hard (density of $250 \, kg/m^3$), we observe erosion of the slab in the lower section of the
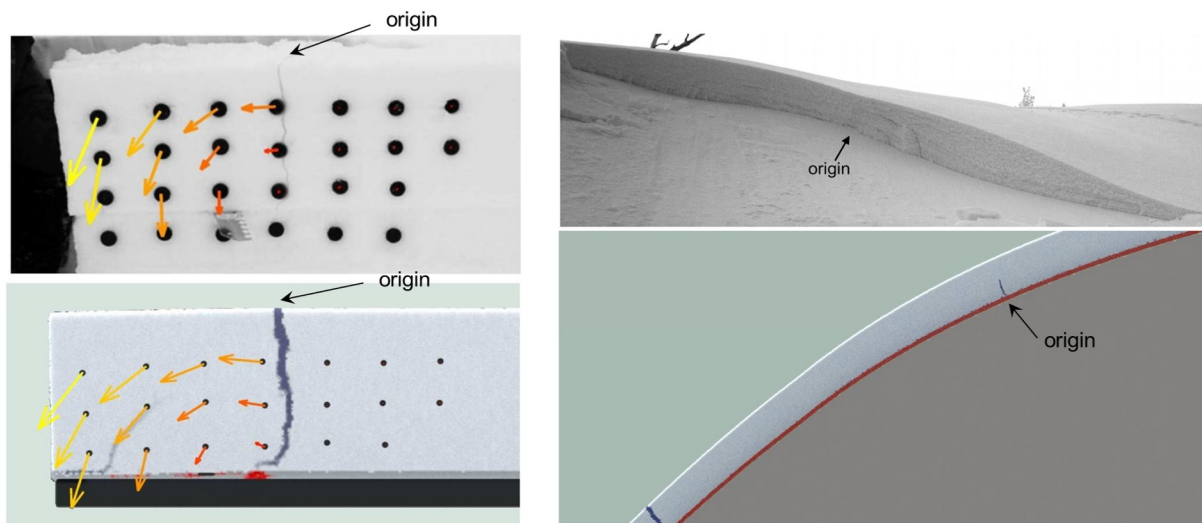

Fig. 5. Differences in slab fracture opening in small scale PST experiments and simulations (left) and in real-scale avalanche crown fracture measurements (Bair et al., 2016) and simulations (right).
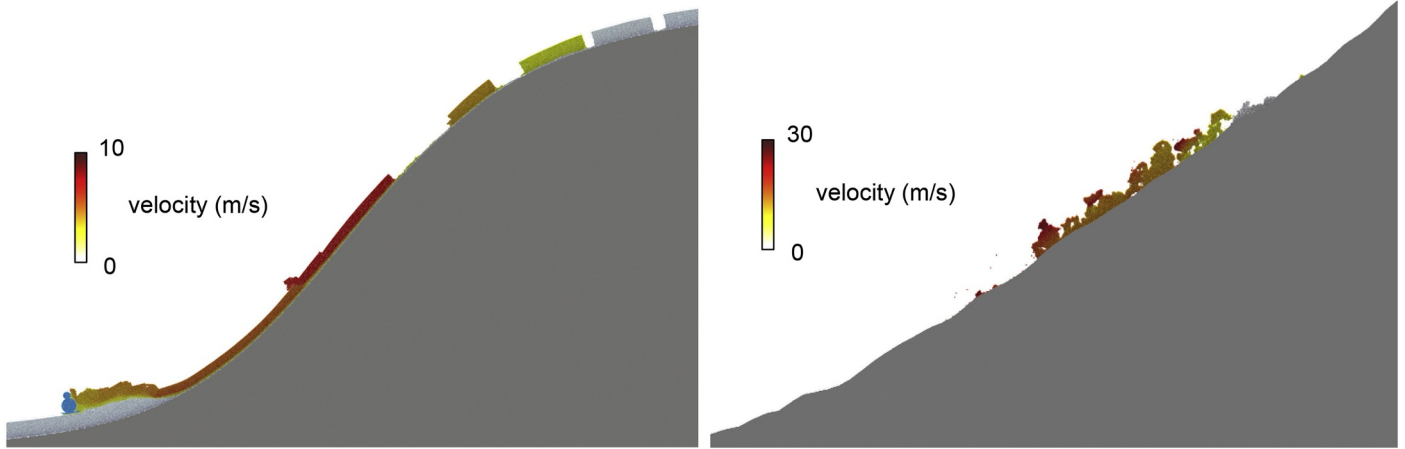
Fig. 6. Left: Flow velocity at the moment of impact of the slab avalanche with the snowman. Right: flow velocity of the 2D flow simulation.

slope (i.e. down-slope the release area) in a sheared zone of 3 to 5 cm thick approximately.

The collective behavior and interactions between broken released slab pieces which collide, split or stick together, leads to a macroscopic fluid-like behavior. For both 2D and 3D simulations (Figs. 1 and 6), we obtained a maximum flow speed $u_m \sim 8$ m/s which is in good agreement with the model and data of McClung and Gauer (2018) ($u_m \sim 1.5 L^{1/2} \sim 2.2 H^{1/2}$). Note that the large 2D simulation with $L = 480$ m and $H = 180$ m (Fig. 6b) led to a maximum flow speed of 27 m/s, again in agreement with the results of McClung and Gauer (2018). In this larger slope simulation (Fig. 6b), we also observed a granulation phenomenon (Steinkogler et al., 2015) which could not be captured in the other simulations due to their limited flow development potential (small path length). For all simulations, we found the α-angle between 20 and 30°, also consistent with McClung and Gauer (2018) (Fig. 7).

4. Discussion

4.1. Shear vs collapse: time to close the debate

The recent studies of Gaume et al. (2015a, 2017a, b, 2018a, b) and Gaume and Reuter (2017) showed that both shear failure and weak layer collapse were required to completely simulate the processes of slab avalanche release. The structural collapse of the weak layer is the only explanation for crack propagation and remote triggering from flat or low angle terrain. However, on steep slopes, typically steeper than 35°, collapse is negligible and the original shear model of McClung (1979) is sufficient to evaluate the conditions for the onset of crack propagation. It is also now clear that the collapse of the weak layer is a secondary process occurring after weak layer has failed. However, observation of different patterns of slab fractures in the field are still feeding this "shear – collapse"
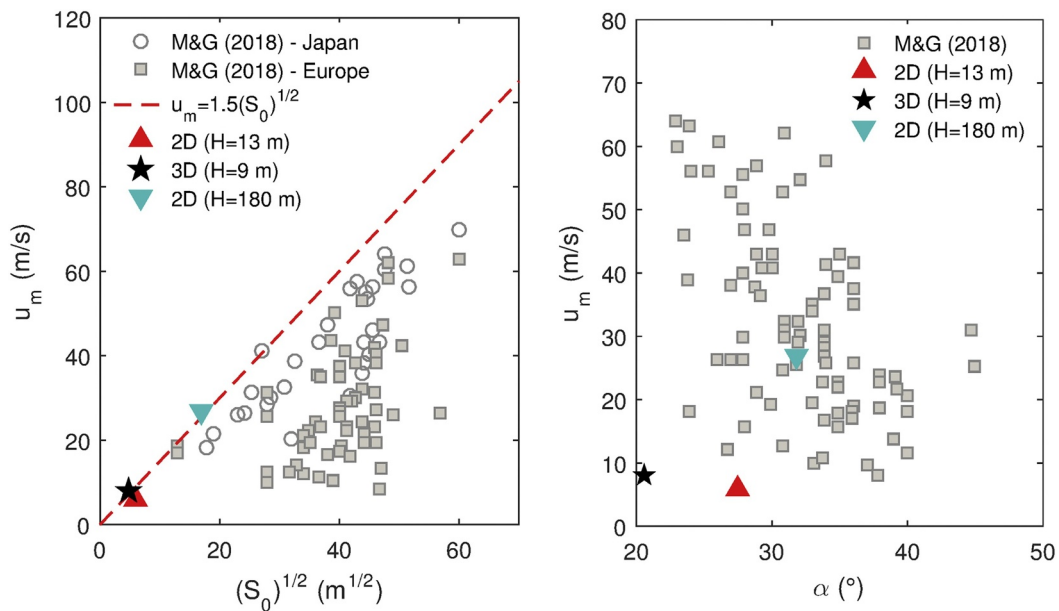

Fig. 7. Left: Maximum velocity during the avalanche flow as a function of the square root of the avalanche length S_0 for the data (Europe and Japan) in McClung and Gauer (2018) and our MPM simulations. Right: Maximum velocity during the avalanche flow as a function of the avalanche α-angle for the data in McClung and Gauer (2018) and our MPM simulations.

debate. Indeed, systematic observations of slab fractures from top to bottom in the Propagation Saw Test tend to justify collapse approaches while observations of real avalanche crown fracture (based on near infrared photogrammetry, Bair et al., 2016; Gauthier et al., 2014) from bottom to top tend to justify pure shear models. Our model which includes both mixed-mode shear-compression failure and weak layer collapse reproduces all these observations and thus reconciles a priori contradictory observations of slab fracture from small scale field tests (top to bottom, Gaume et al., 2018a) and from real avalanches (bottom to top).

4.2. Limitations

One limitation of our model is that the strength of the weak layer is not strain rate dependent. The compaction hardening only depends on the volumetric plastic strain (Eq. 2). Hence, the model can only be used for fast loading cases such as skier triggering or explosives. Ageing processes or sintering (strain-rate dependency of the strength) could be added in the future using the proposal of Barraclough et al. (2018) which would allow to simulate natural avalanche release as well. In addition, apart from the slab depth, the model did not consider the spatial variability of other snowpack parameters which could affect slope stability (Schweizer et al., 2008b; Gaume et al., 2014; Gaume et al., 2015b). Note that spatial variability of slab depth allowed to obtain a realistic release zone inside the simulated domain. Without any source of spatial variability, slab fracture at the flanks would be defined by the boundary condition (Gaume et al., 2018a). Finally, although the release part of the model was validated on small-scale experiments (PST, Gaume et al., 2018a), a direct evaluation of the mechanical parameters of the model based on snow types, density, water content, etc. is still required. Hence, without the ability to predict the snow mechanical behaviour, a complete and rigorous validation of the simulated avalanche dynamics, even with adequate full-scale experimental data, cannot be undertaken.

5. Conclusion

A Material Point Method was applied for snow and avalanche simulations. The model is based on finite strain elastoplasticity and allows to reproduce the complex mechanical behavior of different snow types including weak snowpack layers with a mixed-mode failure followed by strain softening and structural collapse allowing to simulate dynamic anticrack propagation. Simulations of remote triggering and flow of slab avalanches were in good qualitative agreement with field observations. In particular, our simulations reproduce "en-echelon" fractures which have been observed in the field (Gauthier and Jamieson, 2010). Our model contains both ingredients of mixed-mode failure and volumetric collapse and we observe discrepancies in the slab fracture branching mode between PST (top to bottom) and slope-scale (bottom to top) simulations, as observed in the field (Bair et al., 2016). We showed that the propagation speed in avalanche terrain can be 3 to 4 times larger than that measured in PST experiments which could explain different branching mode since fast cracks in the weak layer tend to reduce bending stresses in the slab (Gaume et al., 2015). These larger propagation speeds corroborate field observations of Hamre et al. (2014) who measured speeds larger than 125 m/s based on video recording of full-scale avalanches. Our simulations naturally capture complex phenomena such as snow granulation, erosion and deposition processes without additional implementations. The run-out distance, maximum velocity and α-angles evaluated in our simulations are in good agreement with field data. Our model and results open a promising, but still long route towards operational usage.
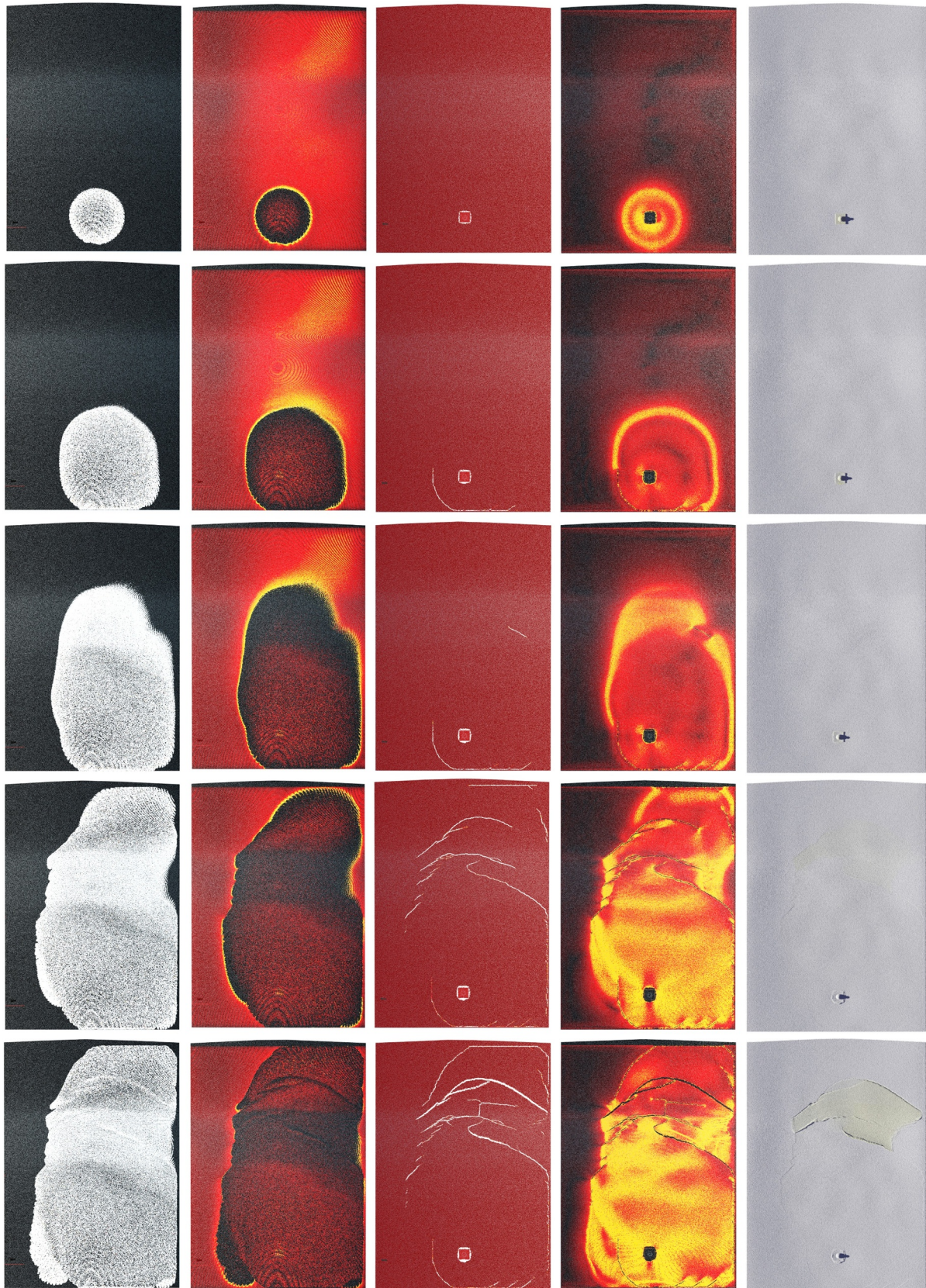
Appendix A. Appendix

Fig. A1. Weak layer and slab states during the release of the avalanche. From left to right: Failed regions in the weak layer (black: elastic; white: failed); First stress invariant p in the weak layer (black to yellow: low to large stress values); Failed regions in the slab (brown: elastic; white: failed); First stress invariant in the slab (black to yellow: low to large stress values); Velocity of slab particles (white to red: low to large velocity values). (For interpretation of the references to colour in this figure legend, the reader is referred to the web version of this article.)
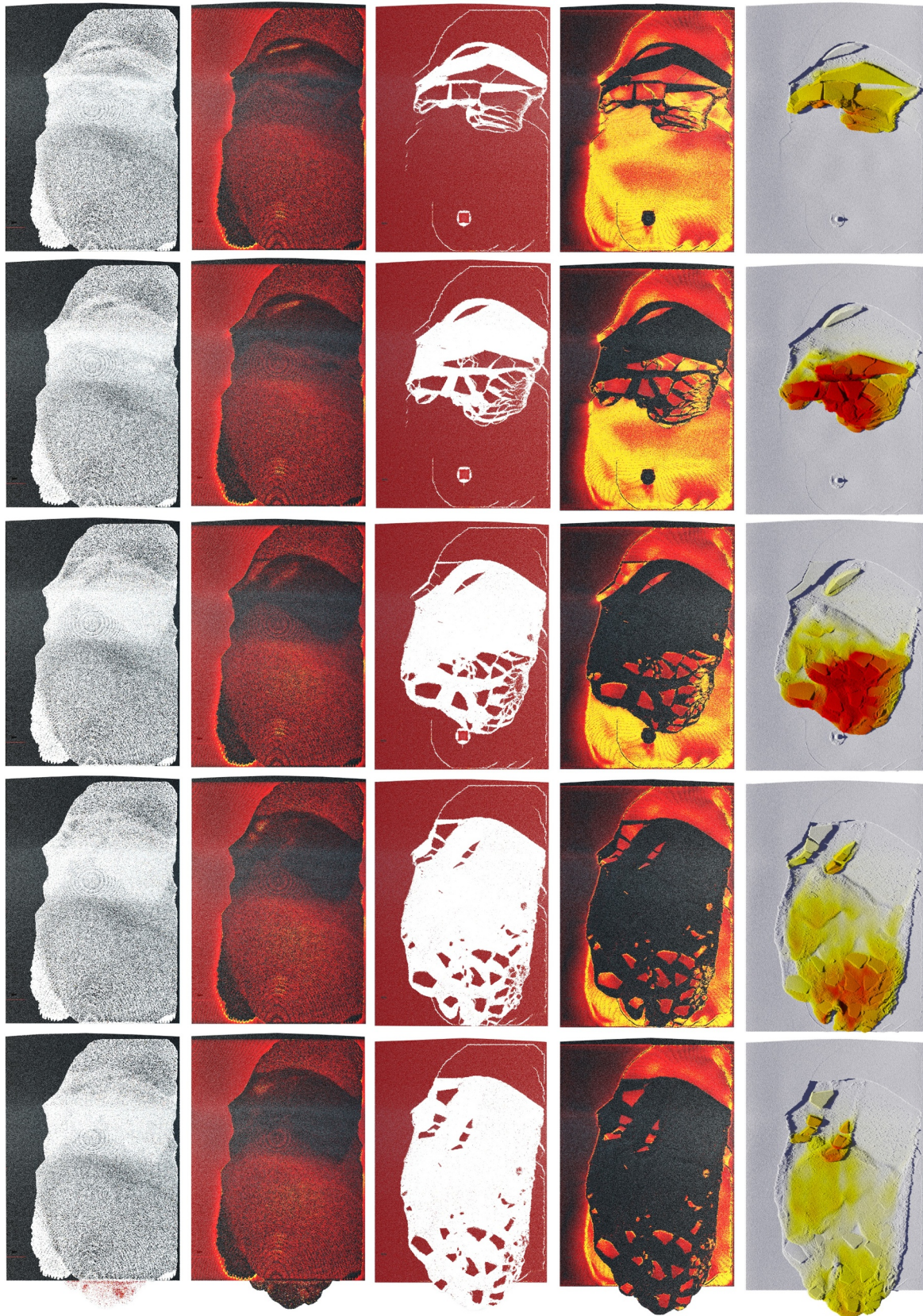
Fig. A2. Weak layer and slab states during the flow of the avalanche. From left to right:: same as A1.

References

Ancey, C., 2018. RAMMS Ou Le Miroir Aux Alouettes. http://www.toraval.ch/ramms-ou-le-miroir-aux-alouettes/.

Ancey, C., Gervasoni, C., Meunier, M., 2004. Computing extreme avalanches. Cold Reg. Sci. Technol. 39 (2–3), 161–180.

Bair, E., Gaume, J., van Herwijnen, A., 2016. The Role of Collapse in Avalanche Release: Review and Implications for Practitioners and Future Research. Proceeding of the ISSW, Breckenridge, CO, pp. 24–31.

Barraclough, T., et al., 2018. Propagating compaction bands in confined compression of snow. Nat. Phys. 13, 272–275.

Bartelt, P., Buser, O., 2018. Avalanche dynamics by newton. reply to comments on avalanche flow models based on the concept of random kinetic energy. J. Glaciol. 64 (243), 165–170.

Benedetti, L., Gaume, J., Fischer, J.T., 2019. A mechanically-based model of snow slab and weak layer fracture in the propagation saw test. Int. J. Solids Struct. 158 (1–20).

Chandel, C., Srivastava, P.K., Mahajan, P., 2015. Determination of failure envelope for faceted snow through numerical simulations. Cold Reg. Sci. Technol. 116, 56–64.

Christen, M., Kowalski, J., Bartelt, P., 2010. RAMMS: numerical simulation of dense snow avalanches in three-dimensional terrain. Cold Reg. Sci. Technol. 63 (1–2), 1–14.

Gauer, P., Kristensen, K., 2016. Four decades of observations from NGI's full-scale avalanche test site Ryggfonn—Summary of experimental results. Cold Reg. Sci. Technol. 125, 162–176.

Gaume, J., Reuter, B., 2017. Assessing snow instability in skier-triggered snow slab avalanches by combining failure initiation and crack propagation. Cold Reg. Sci. Technol. 144, 6–15.

Gaume, J., Schweizer, J., Herwijnen, A., Chambon, G., Reuter, B., Eckert, N., Naaim, M., 2014. Evaluation of slope stability with respect to snowpack spatial variability. J. Geophys. Res. 119 (9), 1783–1799.

Gaume, J., van Herwijnen, A., Chambon, G., Birkeland, K., Schweizer, J., 2015a. Modeling of crack propagation in weak snowpack layers using the discrete element method. Cryosphere 9, 1915–1932.

Gaume, J., Chambon, G., Eckert, N., Naaim, M., Schweizer, J., 2015b. Influence of weak layer heterogeneity and slab properties on slab tensile failure propensity and avalanche release area. Cryosphere 9 (2), 795–804.

Gaume, J., van Herwijnen, A., Chambon, G., Wever, N., Schweizer, J., 2017a. Snow fracture in relation to slab avalanche release: critical state for the onset of crack propagation. Cryosphere 11, 217–228.

Gaume, J., Lowe, H., Tan, S., Tsang, L., 2017b. Scaling laws for the mechanics of loose and cohesive granular materials based on baxter's sticky hard spheres. Phys. Rev. E 96, 032914.

Gaume, J., Gast, T., Teran, J., van Herwijnen, A., Jiang, C., 2018a. Dynamic Anticrack Propagation in Snow. Nat. Commun. 9, 3047.

Gaume, J., Chambon, G., van Herwijnen, A., Schweizer, J., 2018b. Stress concentration in weak snowpack layers and conditions for slab avalanche release. Geophys. Res. Lett. 45 (16), 8363–8369.

Gauthier, D., Jamieson, B., 2010. On the sustainability and arrest of weak layer fracture in whumpfs and avalanches. In: Proceedings of the International Snow Science Workshop, pp. 224–231.

Gauthier, D., Conlan, M., Jamieson, B., 2014. Photogrammetry of Fracture Lines and Avalanche Terrain: Potential Applications to Research and Hazard Mitigation Projects. Proceeding of the ISSW, Banff, CA, pp. 109–115.

Hagenmuller, P., 2017. Microstructure-based finite element modeling of snow failure envelope. Geophys. Res. Abstr. 19, 4459.

Hagenmuller, P., Chambon, G., Naaim, M., 2015. Microstructure-based modeling of snow mechanics: a discrete element approach. Cryosphere 9 (5), 1969–1982.

Hamre, D., Simenhois, R., Birkeland, K., 2014. Fracture Speed of Triggered Avalanches. In Proceedings ISSW 2014, pp. 174–178 Banff.

Harbitz, C.B., Issler, D., Keylock, C.J., 1998. Conclusions from a recent survey of avalanche computational models. In: Proceedings of the Anniversary Conference. vol. 25. pp. 128–135.

Heierli, J., Gumbsch, P., Zaiser, M., 2008. Anticrack nucleation as triggering mechanism for snow slab avalanches. Science 321, 240–243.

Helbig, N., van Herwijnen, A., Magnusson, J., Jonas, T., 2015. Fractional snow-covered area parameterization over complex topography. Hydrol. Earth Syst. Sci. 19 (3), 1339–1351.

Issler, D., Jenkins, J.T., McElwaine, J.N., 2018. Comments on avalanche flow models based on the concept of random kinetic energy. J. Glaciol. 64 (243), 148–164.

Jamieson, B., Margreth, S., Jones, A., 2008. Application and limitations of dynamic models for snow avalanche hazard mapping. In: Proceedings Whistler 2008 International Snow Science Workshop September 21–27. 2008. pp. 730.

Jiang, C., Schroeder, C., Teran, J., Stomakhin, A., Selle, A., 2016. The material point method for simulating continuum materials. In: ACM SIGGRAPH 2016 Course, pp. 1–52.

Köhler, A., McElwaine, J.N., Sovilla, B., Ash, M., Brennan, P., 2016. The dynamics of surges in the 3 February 2015 avalanches in Vallée de la Sionne. J. Geophys. Res. 121 (11), 2192–2210.

Köhler, A., Fischer, J.T., Scandroglio, R., Bavay, M., McElwaine, J., Sovilla, B., 2018. Cold-to-warm flow regime transition in snow avalanches. Cryosphere 12 (12), 3759–3774.

Louchet, F., Duclos, A., Caffo, S., 2013. Modeling a Fluid/Solid Transition in Snow Weak Layers Application to Snow Avalanche Release. Proceeding of the ISSW, Grenoble, France, pp. 270–277.

McClung, D., 1979. Shear fracture precipitated by strain softening as a mechanism of dry slab avalanche release. J. Geophys. Res. 84 (B7), 3519–3526.

McClung, D.M., Gauer, P., 2018. Maximum frontal speeds, alpha angles and deposit volumes of flowing snow avalanches. Cold Reg. Sci. Technol. 153, 78–85.

Mulak, D., Gaume, J., 2019. Numerical investigation of the mixed-mode failure of snow. Computat. Part. Mech. 1–9.

Perla, R.I., 1971. The Slab Avalanche. vol. 100 University of Utah, Salt Lake City.

Perlin, K., 2002. Improving noise. In: ACM Transactions on Graphics (TOG). 21. pp. 681–682 3.

Podolskiy, E.A., Chambon, G., Naaim, M., Gaume, J., 2013. A review of finite-element modelling in snow mechanics. J. Glaciol. 59 (218), 1189–1201.

Reiweger, I., Schweizer, J., 2010. Failure of a layer of buried surface hoar. Geophys. Res. Lett. 37 (24).

Reiweger, I., Gaume, J., Schweizer, J., 2015. A new mixed-mode failure criterion for weak snowpack layers. Geophys. Res. Lett. 42, 1427–1432.

Reuter, B., Schweizer, J., 2018. Describing snow instability by failure initiation, crack propagation, and slab tensile support. Geophys. Res. Lett. 45 (14), 7019–7027.

Schweizer, J., 1999. Review of dry snow slab avalanche release. Cold Reg. Sci. Technol. 30 (1–3), 43–57.

Schweizer, J., 2017. On recent advances in avalanche research. Cold Reg. Sci. Technol. 144, 1–5.

Schweizer, J., Jamieson, B., Schneebeli, M., 2003. Snow avalanche formation. Rev. Geophys. 41 (4), 1016.

Schweizer, J., McCammon, I., Jamieson, J.B., 2008. Snowpack observations and fracture concepts for skier-triggering of dry-snow slab avalanches. Cold Reg. Sci. Technol. 51 (2–3), 112–121.

Schweizer, J., Kronholm, K., Jamieson, J.B., Birkeland, K.W., 2008b. Review of spatial variability of snowpack properties and its importance for avalanche formation. Cold Reg. Sci. Technol. 51 (2–3), 253–272.

Schweizer, J., Reuter, B., van Herwijnen, A., Gaume, J., 2016. Avalanche Release 101. Proceeding of the ISSW. Breckenridge, CO. pp. 1–10.

Srivastava, P., Chandel, C., Mahajan, P., 2017. Micromechanical modeling of elastic and strength properties of snow. In: SLAM3 - Slab Avalanche Multiscale Mechanical Modeling, pp. 12–13 Davos, Switzerland.

Steinkogler, W., Gaume, J., Löwe, H., Sovilla, B., Lehning, M., 2015. Granulation of snow: from tumbler experiments to discrete element simulations. J. Geophys. Res. 120 (6), 1107–1126.

Stomakhin, A., Schroeder, C., Chai, L., Teran, J., Selle, A., 2013. A material point method for snow simulation. ACM Trans. Graph. 32 (4), 102.

Sulsky, D., Zhou, S.-J., Schreyer, H.L., 1995. Application of a particle-in-cell method to solid mechanics. Comput. Phys. Commun. 87, 236–252.

van Herwijnen, A., Jamieson, B., 2005. High-speed photography of fractures in weak snowpack layers. Cold Reg. Sci. Technol. 43 (1–2), 71–82.

van Herwijnen, A., Schweizer, J., Heierli, J., 2010. Measurement of the deformation field associated with fracture propagation in weak snowpack layers. J. Geophys. Res. 115 (F3).

van Herwijnen, A., Gaume, J., Bair, E.H., Reuter, B., Birkeland, K.W., Schweizer, J., 2016. Estimating the effective elastic modulus and specific fracture energy of snowpack layers from field experiments. J. Glaciol. 62 (236), 997–1007.

van Herwijnen, A., Bair, E.H., Birkeland, K.W., Reuter, B., Simenhois, R., Jamieson, B., Schweizer, J., 2016b. Measuring the mechanical properties of snow relevant for dry-snow slab avalanche release using particle tracking velocimetry. In: Proceedings ISSW, pp. 397–404.